Supplementary Information

The role of hydrophobic modification on hyaluronic acid dynamics and self-assembly

William M. Payne,[a,‡] *Denis Svechkarev,*[a,‡] *Alexander Kyrychenko,*[b] *Aaron M. Mohs*[a,c,d*]

[a]Department of Pharmaceutical Sciences, University of Nebraska Medical Center
986858 Nebraska Medical Center, Omaha, NE 68198-6858, United States

[b]Institute for Chemistry, V. N. Karazin Kharkiv National University
4 Svobody Square, 61022 Kharkiv, Ukraine

[c]Fred and Pamela Buffett Cancer Center, University of Nebraska Medical Center, 986858 Nebraska Medical Center, Omaha, NE 68198-6858, United States

[d]Department of Biochemistry and Molecular Biology, University of Nebraska Medical Center, 986858 Nebraska Medical Center, Omaha, NE 68198-6858, United States

1. Placement of hydrophobic ligands and dissociated carboxylates for simulations

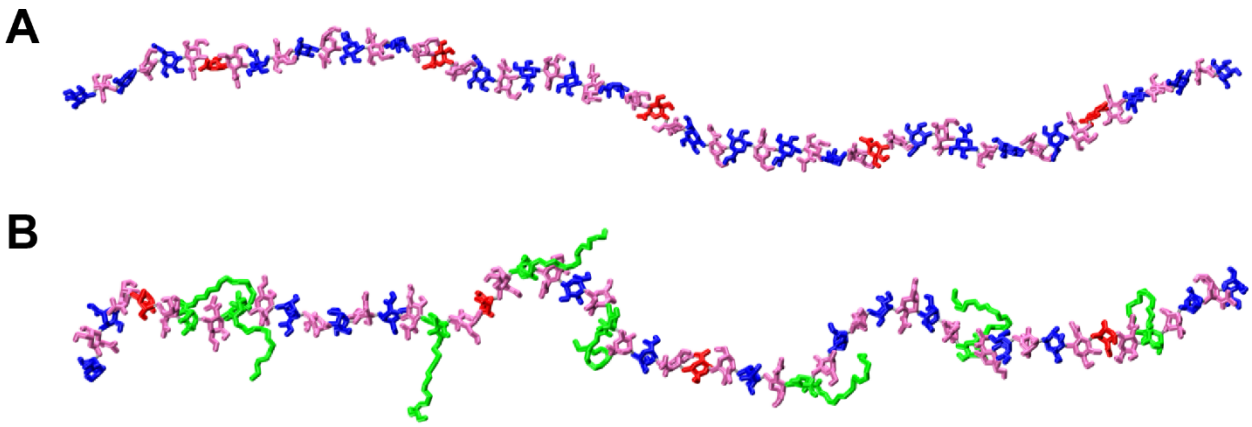

Figure S1. Visual schematic of the HA modification for simulations. **(A)** shows the placement of deprotonated glucuronic acid (red) and protonated glucuronic acid (blue) for the 50% dissociated HA model. N-acetylglucosamine is colored mauve for reference. **(B)** shows the placement of hydrophobically modified glucuronic acid moieties chosen at random (green) with unmodified, protonated glucuronic acid moieties (blue) and unprotonated glucuronic acid moieties (red). N-acetlyglucosamine moieties are shown in mauve.

2. Graphical representation of polymer compaction

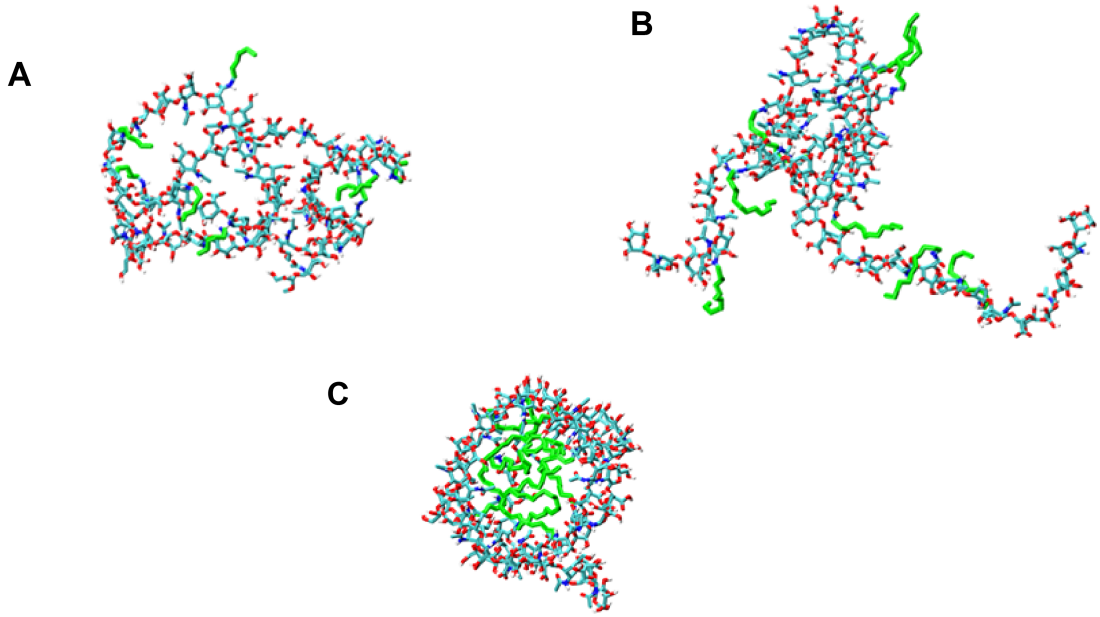

Figure S2. Hydrophobically modified HA polymer conformations after 260 ns of simulation. **(A)** shows the conformation of hexHA, which appears compact but does not form a distinct hydrophobic core. The conformation of dodHA **(B)** is much less compact and defined than ocdHA **(C)** which exhibits a well-defined hydrophobic core.

3. Analysis of glycosidic dihedral angles dynamics

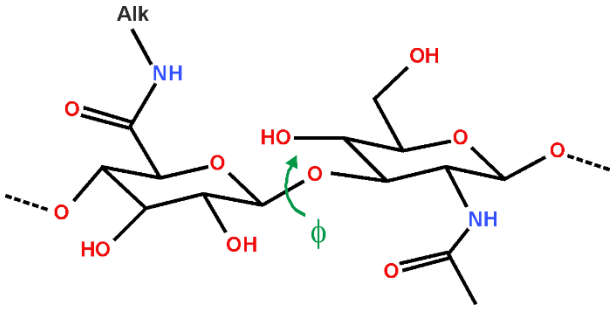

Scheme S1. Schematic illustrating the dihedral angle that was analyzed for all samples.

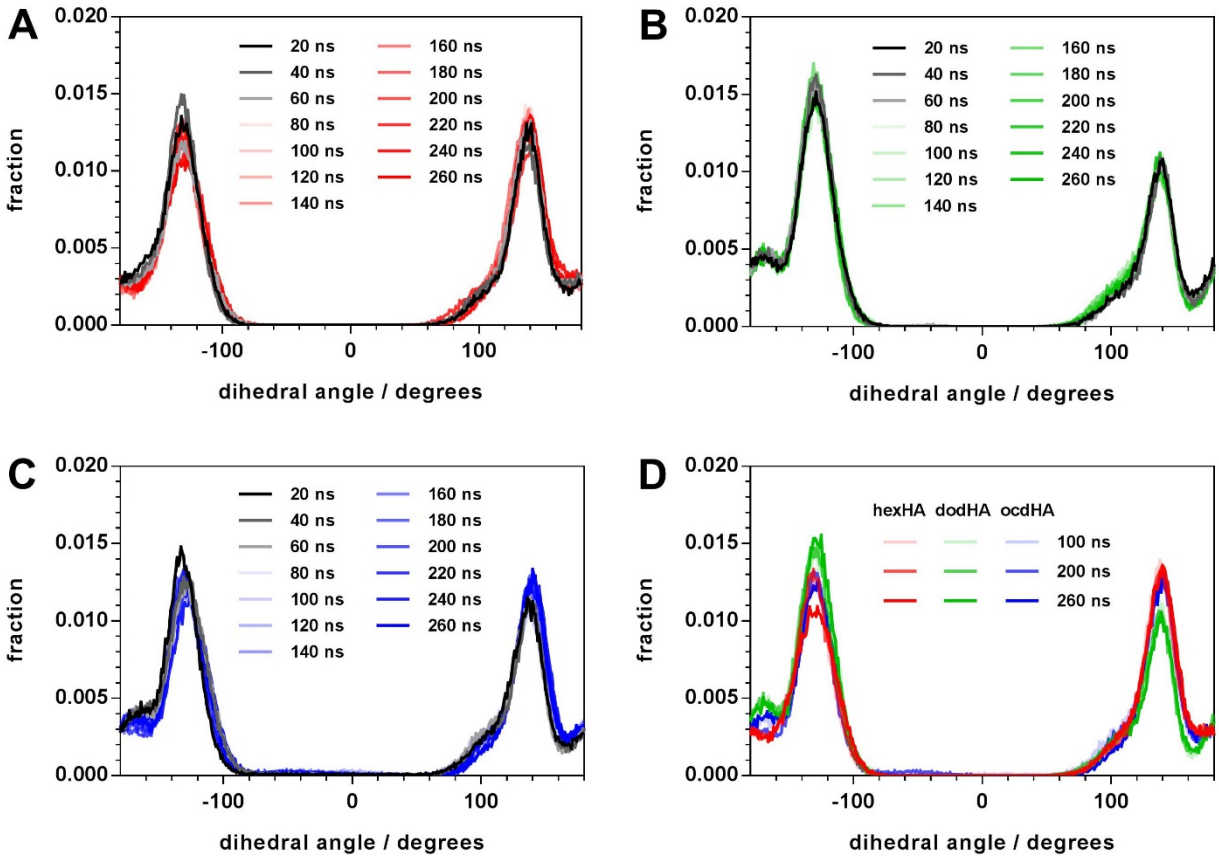

Figure S3. Distribution of the dihedral angles for **(A)** hexHA, **(B)** dodHA, **(C)** ocdHA, and **(D)** comparison between the distribution of the dihedral angles for all three derivatives at 100, 200 and 260 ns. No significant difference is noticed, and all glycosidic dihedral angles values fluctuate around ±120°.

4. Simulation reproduction of hydrophobically-modified HA derivatives

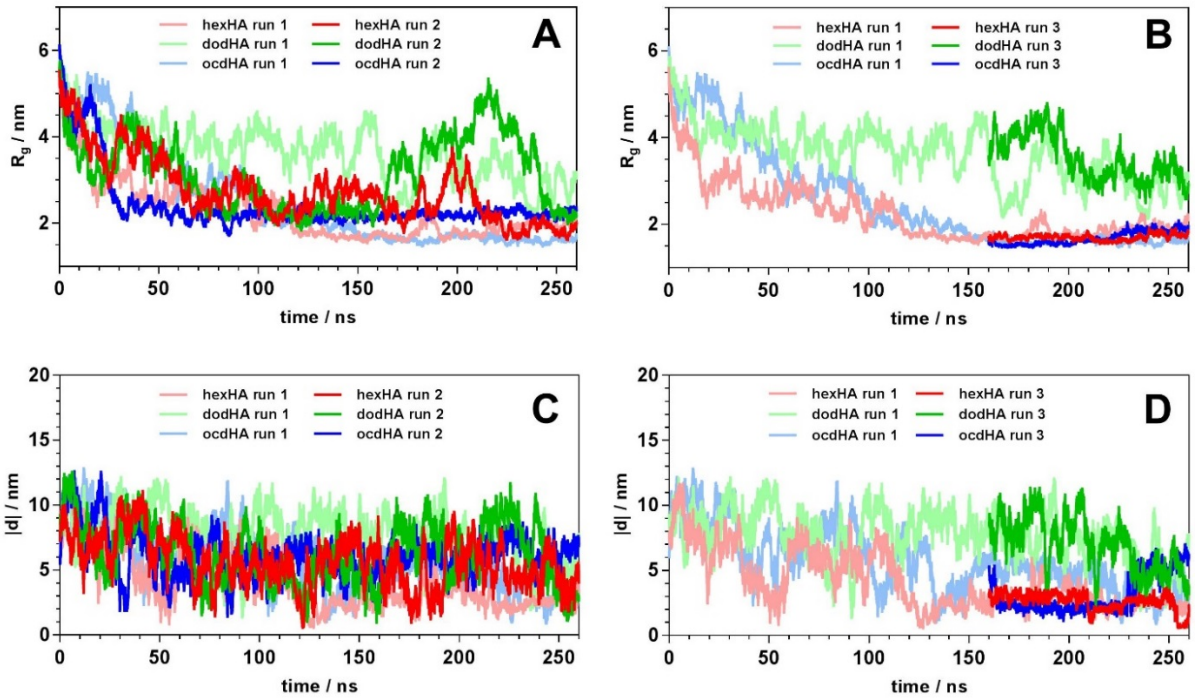

Figure S4. Additional simulations of hydrophobically modified HA. **(A), (B)** show the change in radius of gyration along the simulation trajectories. **(C), (D)** show the change in head-to-tail distance along the simulation trajectories. Run 1 is the initial simulation represented and discussed in the main text. Run 2 is an additional independent simulation performed using the initial linear configurations of the polymers (the same starting geometries that were used for Run 1). Run 3 is an independent simulation using the equilibrated polymer configurations from the Run 1 at 160 ns. The hexyl and octadecyl derivatives coincide with the behavior observed in Run 1 closely. In Run 2, the dodecyl HA tends to be more compact than in Run 1; however, at a later stage it exhibits further partial disassembly. Being restarted from the intermediate equilibrated configurations from Run 1, all three systems closely follow their behavior observed in earlier simulation. Overall, we can conclude that the dodecyl HA exhibits higher instability in self-assembly behavior that potentially leads to less tightly packed nanoaggregates of larger sizes.

5. Simulations of 50% substituted HA derivatives

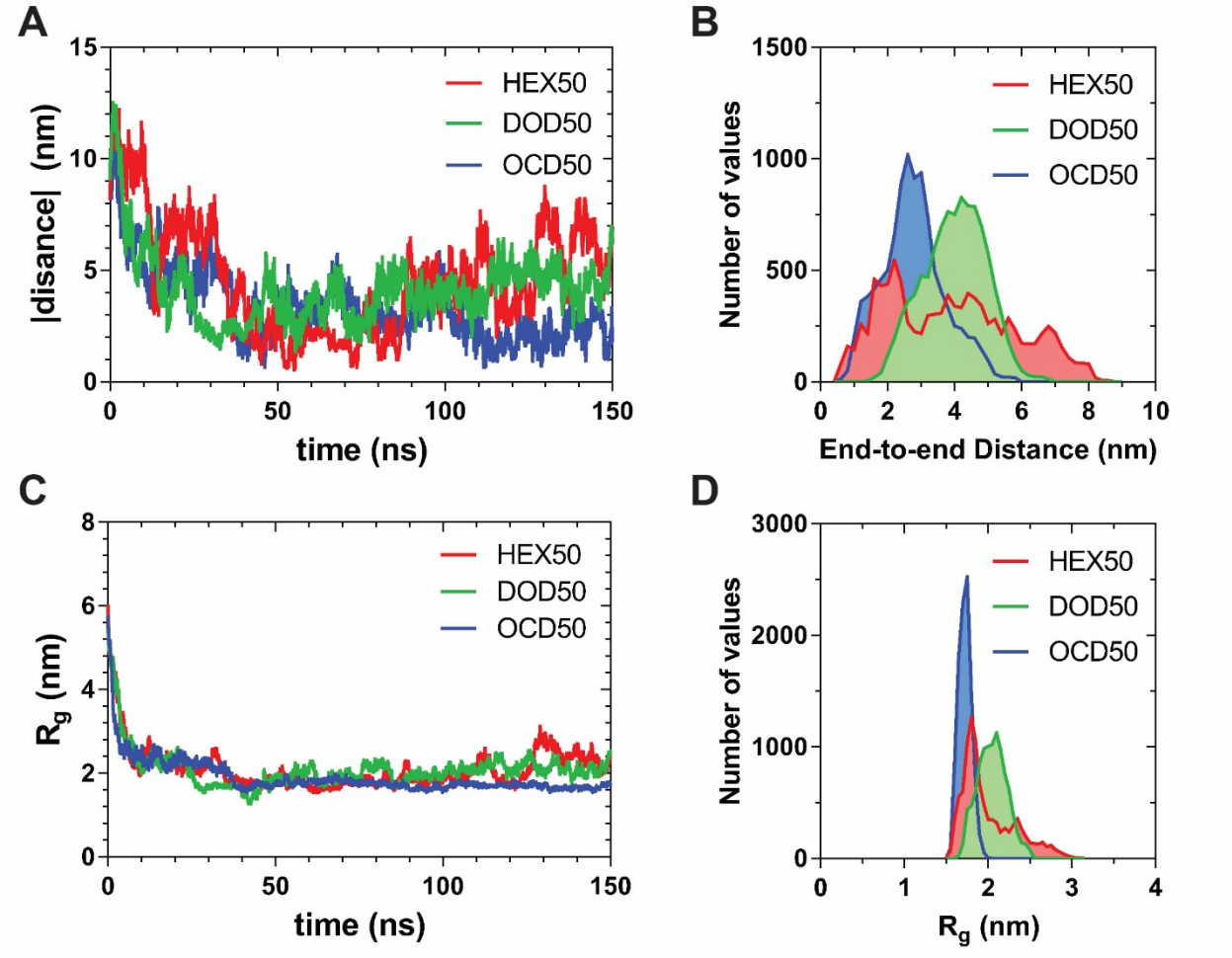

Figure S5. To evaluate if the substitution ratio affects the polymer behavior *in silico*, models of HA amphiphiles were constructed with 50% substitution with alkyl chains. Simulations were performed for 150 nanoseconds, and distributions of the values were taken between 50-150 ns to compare to Figure 2. **(A)** shows the end-to-end distance data from the simulation results, and the distribution of samplings from 50-150 ns are shown in **(B)**. The radius of gyration quickly reaches a stable state **(C)**, and the samplings from 50-150 ns are shown in **(D)**. The more substituted HA derivatives shown here reach a stable radius of gyration more quickly than the less substituted derivatives shown in Figure 2. However, the same trends observed for the less substituted HA amphiphiles are observed with their 50% substituted analogs.

6. NMR Determinations of the degree of alkyl substitution in HA derivatives

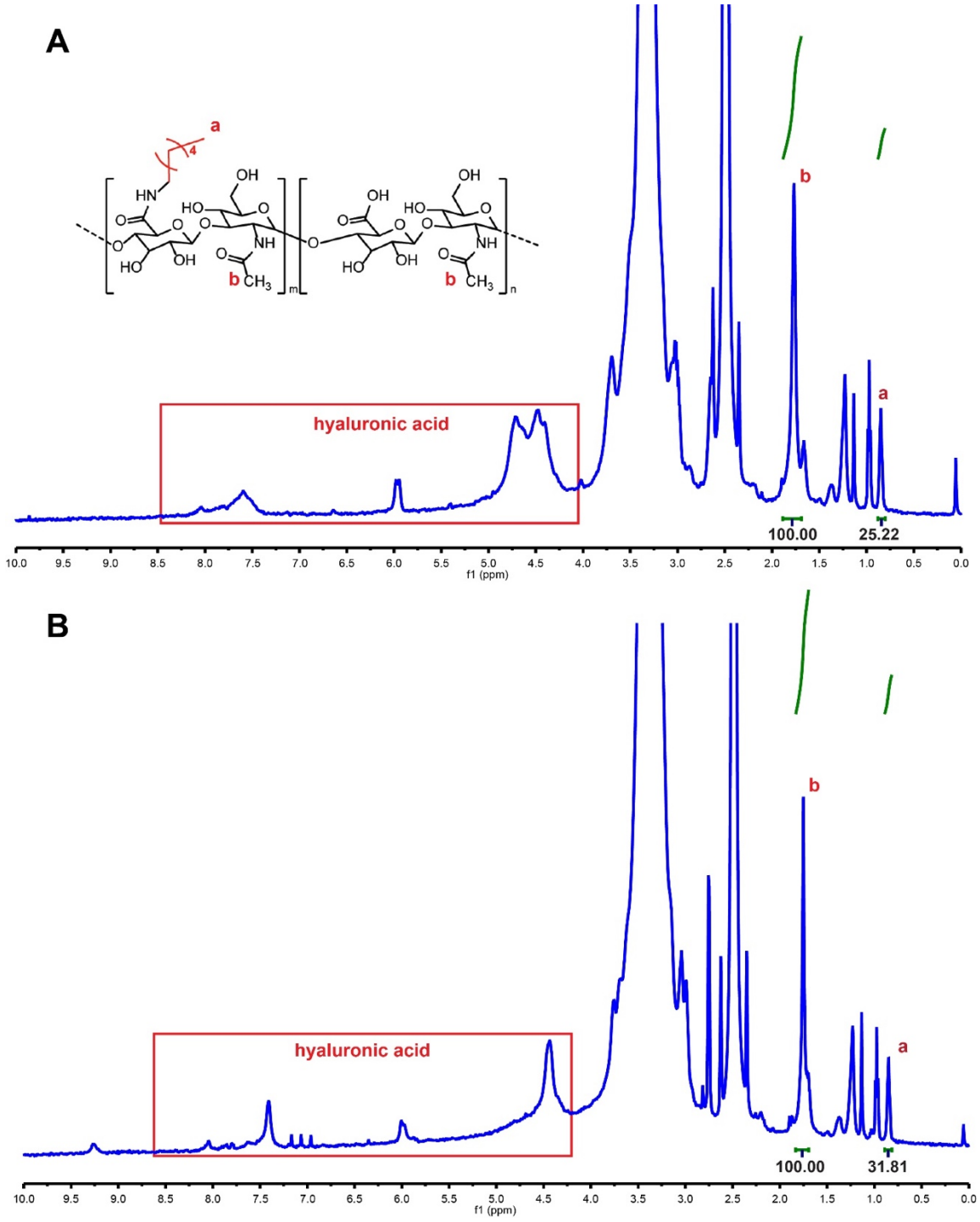

Figure S6. NMR of hexylamine-modified HA samples. **(A)** shows the results from 10 kDa hexHA and **(B)** shows the results of 100 kDa hexHA. Data was processed in Mnova software to calculate molar conjugation ratios and is reported in Table S1.

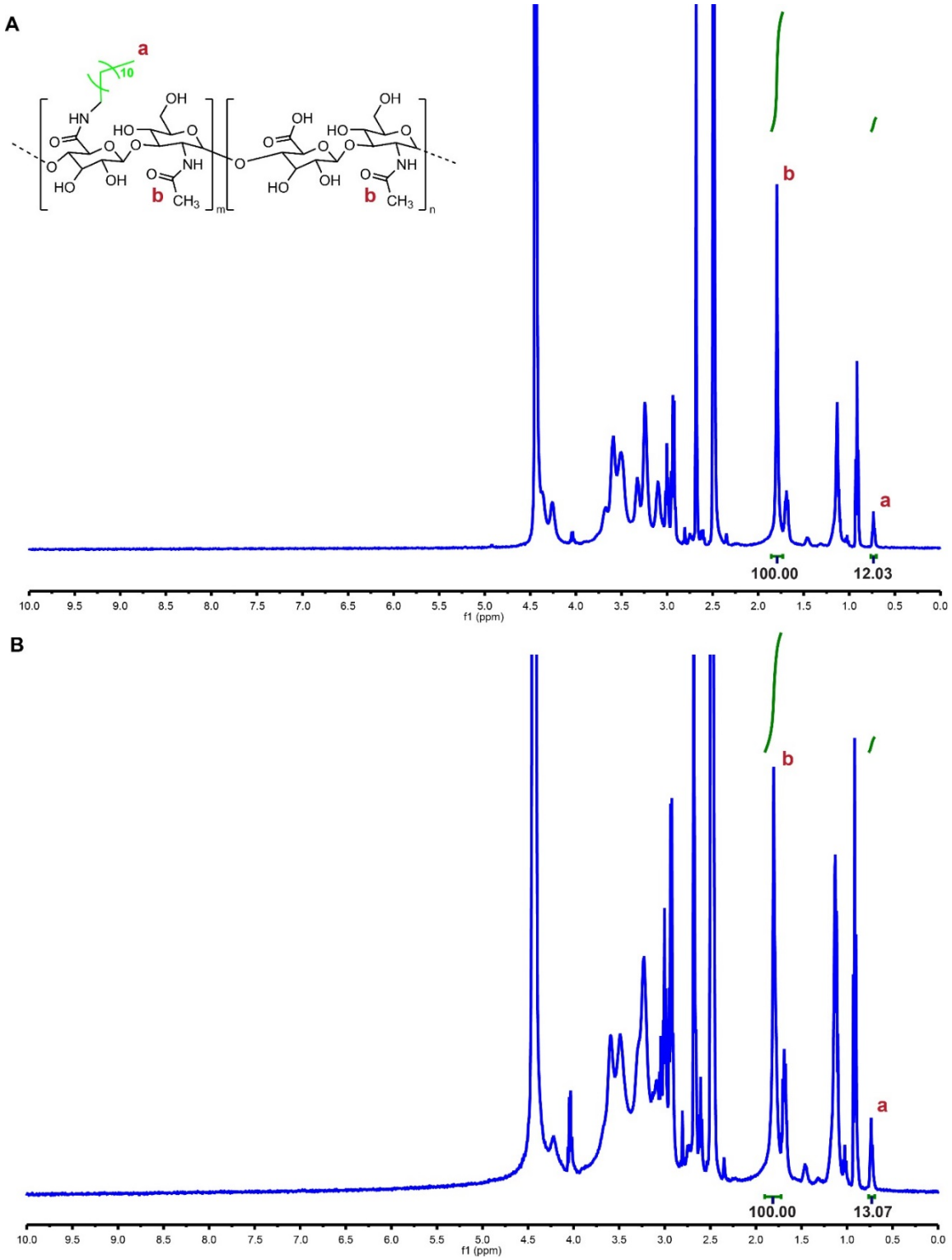

Figure S7. NMR of dodecylamine-modified HA. **(A)** shows the NMR spectrum for 10 kDa dodHA and **(B)** shows the NMR spectrum for 100 kDa dodHA. Results are summarized in Table S1.

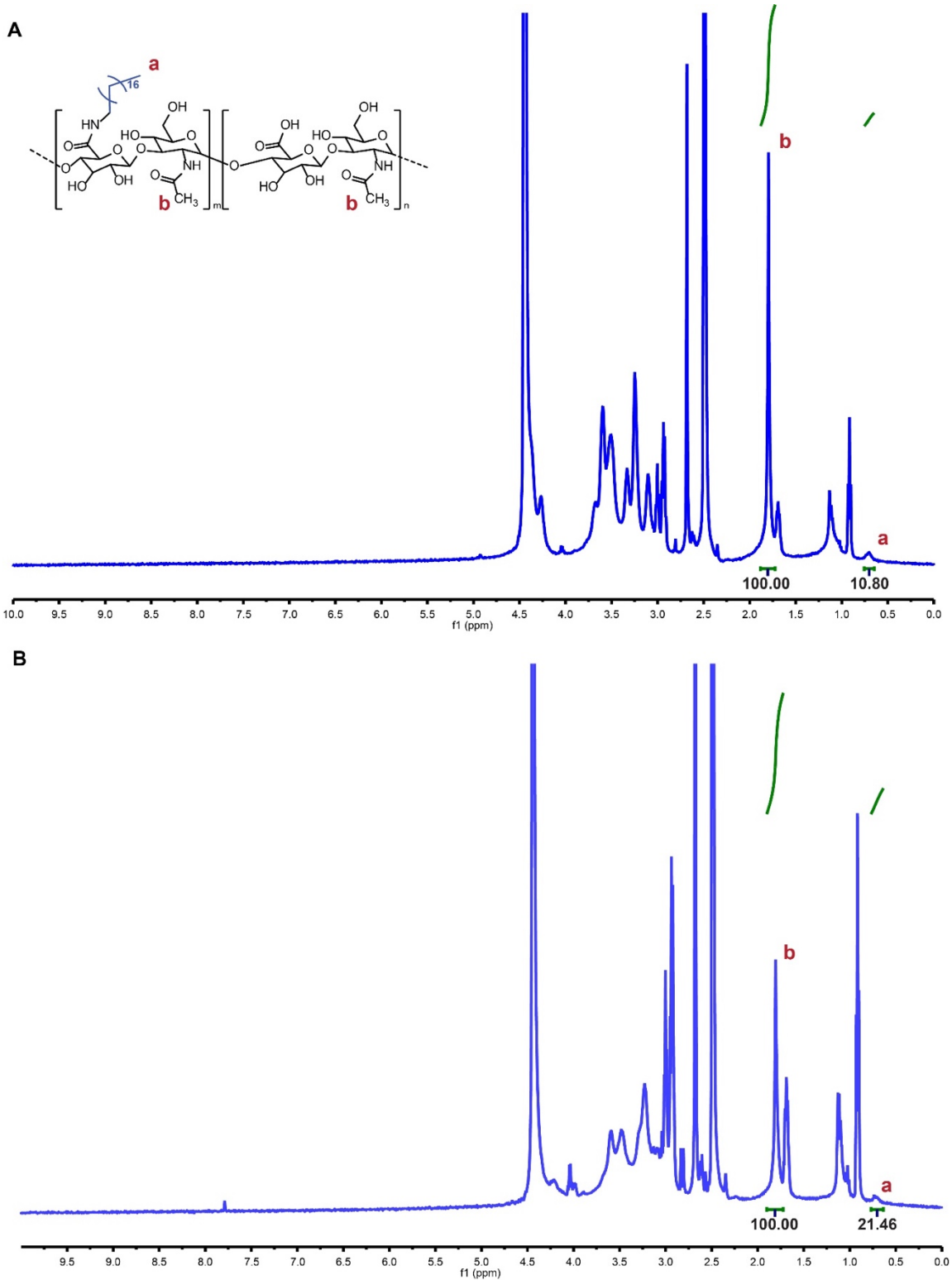

Figure S8. NMR spectra of octadecylamine-modified HA. **(A)** shows the NMR spectrum for 10 kDa ocdHA, and **(B)** shows the NMR spectrum of 100 kDa HA. The results are summarized in Table S1.

Table S1. Molar ratios of alkyl chains to hyaluronic acid calculated from NMR analysis. Ratios were calculated from NMR peaks as described by Hill, et al [Hill, et al., 2015].

Conjugate	HA Molecular Weight	
	10 kDa	**100 kDa**
hexHA	25.22%	31.81%
dodHA	12.03%	13.07%
ocdHA	10.80%	21.46%

REFERENCES:

Hill, T. K., Abdulahad, A., Kelkar, S. S., Marini, F. C., Long, T. E., Provenzale, J. M., & Mohs, A. M. (2015). Indocyanine Green-Loaded Nanoparticles for Image-Guided Tumor Surgery. *Bioconjugate Chemistry*, *26*(2), 294–303. http://doi.org/10.1021/bc5005679